

Contents lists available at ScienceDirect

#### Petroleum Science

journal homepage: www.keaipublishing.com/en/journals/petroleum-science



#### Original Paper

# Synergistic stabilization of emulsions by microspheres and surfactants for enhanced oil recovery



Yu-Hui Yang <sup>a, b</sup>, Chu-Yu Kang <sup>a</sup>, Ting-Feng Liu <sup>c</sup>, Hang Li <sup>a</sup>, Hui-Min Yu <sup>a</sup>, Zhuo-Zhuang Liu <sup>a</sup>, Hai-Ming Fan <sup>a, b, \*</sup>

- <sup>a</sup> College of Petroleum Engineering, China University of Petroleum (East China), Qingdao, 266580, Shandong, PR China
- <sup>b</sup> Shandong Key Laboratory of Oil and Gas Field Chemistry, Qingdao, 266580, Shandong, PR China
- <sup>c</sup> Shengli Oilfield Petroleum Engineering Technology Research Institute, Dongying, 257100, Shandong, PR China

#### ARTICLE INFO

# Article history: Received 1 October 2024 Received in revised form 26 March 2025 Accepted 28 March 2025 Available online 28 March 2025

Edited by Yan-Hua Sun

Keywords:
Microsphere
Inverse microemulsion polymerization
Surfactant oil displacement
Emulsion stability
Enhanced oil recovery

#### ABSTRACT

During oil displacement, surfactants often encounter challenges such as emulsion instability and channeling, which can compromise their efficiency. To address these issues, polymer microspheres were synthesized via reverse microemulsion polymerization using acrylamide, acrylamidopropane sulfonic acid, and stearyl methacrylate as monomers, with N,N-methylenebisacrylamide as the crosslinker. The microspheres were then combined with sodium alkyl alcohol polyoxyethylene ether carboxylate to enhance emulsion stability and expand the swept volume of surfactant. A stable reverse microemulsion system was prepared using the maximum water solubilization rate as the indicator, and microspheres were synthesized based on this system. The ability of the microspheres to enhance emulsion stability was systematically evaluated. The plugging performance and enhanced oil recovery (EOR) efficiency of the microsphere/surfactant composite system were assessed through core seepage and oil displacement experiments. The experimental results demonstrated that microspheres were successfully prepared in a water-in-oil reverse microemulsion system with a solubilization rate of 42%. The emulsion stability was evaluated under an oil-to-water ratio of 7:3, a temperature of 80 °C, and a salinity of 44,592 mg/L, by manually shaking the test tube five times. It was observed that the complete phase separation time of the emulsion increased from 10 to 120 min after the addition of microspheres. Under different permeability conditions (100  $\times$  10<sup>-3</sup>, 300  $\times$  10<sup>-3</sup>,  $500 \times 10^{-3} \, \mu \text{m}^2$ ), the recovery efficiency of the composite system increased by 4.5%, 8.3%, and 4.8%, respectively, compared to a single surfactant system. The microspheres developed in this study enhanced emulsion stability and increased the swept volume of surfactant within the formation, significantly boosting its oil recovery efficiency.

© 2025 The Authors. Publishing services by Elsevier B.V. on behalf of KeAi Communications Co. Ltd. This is an open access article under the CC BY license (http://creativecommons.org/licenses/by/4.0/).

#### 1. Introduction

As oilfield development progresses, the focus has moved from reservoirs with favorable geological conditions, which are mostly depleted, to medium-to-low permeability reservoirs that are characterized by high temperatures and high salinity (Chen et al., 2023; Fan et al., 2023; Liu et al., 2021; Lu et al., 2014; Zhao et al., 2021). These reservoirs exhibit low permeability, elevated temperatures, high salinity, and pronounced geological heterogeneity, leading to frequent water channeling and low recovery rates after

water flooding. As a result, over 70% of the residual oil typically remains trapped underground (Baek et al., 2019; Liu et al., 2022; Saha et al., 2018, 2019; Shang et al., 2019). Surfactants can form emulsions under shear conditions within the reservoir. These emulsions enhance the oil—water mobility ratio through the Jamin effect, which improves the sweep efficiency of the displacing phase and effectively reduces the channeling of small-molecule oil displacement agents (Dantas et al., 2020; Lee et al., 2020; Li G. et al., 2019; Sharma et al., 2023; Zhou et al., 2022). This approach offers considerable potential for application in heterogeneous, medium-to-low permeability reservoirs. However, under high-temperature, high-salinity, and unstable shear flow conditions, the stability of the emulsion is often compromised (Arab et al., 2018; Kumar et al., 2021).

E-mail address: haimingfan@126.com (H.-M. Fan).

<sup>\*</sup> Corresponding author.

Combining surfactants or incorporating alkaline agents can improve their emulsification performance. For instance, Hou and Sheng (2022) developed a surfactant system with excellent sponemulsification properties by combining cetyltrimethylammonium bromide with nonylphenol ethoxylate carboxvlate and incorporating 0.1% NaOH into the system. This formulation enables emulsification with just a single inversion of the small bottle containing the oil-water mixture (Hou and Sheng, 2022). Jiang et al. (2021) developed a spontaneous emulsification system by combining hydrophobic-modified polyvinyl alcohol (HPVA) with cetyltrimethylammonium bromide (CTAB). When the concentration reached 3000 mg/L and the mass ratio of HPVA to CTAB was 7:3, the dynamic interfacial tension between oil and water dropped to an ultra-low level (Jiang et al., 2021). Li Z. et al. (2019) developed a surfactant system with spontaneous emulsification capabilities by combining anionic alkyl polyglucoside hydroxypropyl sulfonate sodium with cetyltrimethylammonium bromide. This system allows for oil-water emulsification with just a single inversion, producing droplets with a size as small as 0.2 μm (Li et al., 2019). Liu et al. (2022) developed a viscous oil viscosity-reducing system with excellent emulsification properties by combining primary alcohol ethoxylate ester (0.25%), sodium dodecyl sulfate (0.25%), and NaOH (0.05%). This system achieves ultra-low interfacial tension, with the droplet size of the emulsified viscous oil reaching as small as 0.2 µm (Liu et al., 2022). Shang et al., 2019 developed a surfactant/alkaline flooding system by combining monoethanolamine (MEA) and sodium carbonate (Na<sub>2</sub>CO<sub>3</sub>) with sulfonate surfactants (0.20% SLPS + 0.15% Na<sub>2</sub>CO<sub>3</sub> + 0.10% MEA). This system exhibits strong salt tolerance and can reduce the oil-water interfacial tension (IFT) to ultra-low levels (<10<sup>-3</sup> mN/m) under conditions of NaCl concentration below 40,000 mg/L, CaCl<sub>2</sub> concentration below 400 mg/L, and temperatures below 90 °C (Shang et al., 2019). However, during the later stages of extraction, preferential flow paths created by prolonged water injection and the formation heterogeneity (e.g., natural microfractures in low-permeability media) may cause the spontaneous emulsification system to prematurely break through before reaching the oil, potentially diminishing its effectiveness in improving oil recovery. Furthermore, the addition of alkali could also heighten the risk of scaling in the formation (An et al., 2022; Bai et al., 2017; Wang et al., 2019).

Microspheres are particle-type gels formed through polymer cross-linking, offering adjustable particle sizes, excellent dispersion, and injectability. They have been widely utilized in oilfields to enhance oil recovery (Li et al., 2022; Ma et al., 2022; Wang et al., 2022; Zheng et al., 2022; Zhou et al., 2023). Wang et al. (2020) developed a composite oil recovery system incorporating microspheres and surfactants. Experimental results show that this system significantly reduces water breakthrough in high-permeability channels and provides effective profile control and enhanced oil recovery efficiency (Wang et al., 2020). Zhu et al. (2022) developed an environmentally friendly polymer microsphere and created an eco-friendly polymer microsphere/surfactant composite system. Following water flooding, the injection of this composite system resulted in a 10.1% increase in oil recovery (Zhu et al., 2022). These findings suggest that combining microspheres with surfactants can extend the sweep efficiency of surfactant and improve its oil recovery effectiveness.

Existing microsphere/surfactant composite systems for improving oil recovry mainly leverage the profile control capability of microsphere plugs to mitigate surfactant channeling in highly heterogeneous formations. This approach enhances the surfactant sweep efficiency and improves oil recovery. Our study demonstrates that mixing the microspheres with surfactants not only mitigate surfactant channeling but also enhances the stability of the emulsion under low shear conditions and improves the

emulsification capacity of surfactant for crude oil. This study specifically utilizes inverse microemulsion polymerization to fabricate microspheres and optimizes their synthesis conditions with cost considerations in mind. The primary focus is on evaluating how the microspheres enhance emulsion stability and assessing the effectiveness of the microsphere/surfactant composite system in improving oil recovery. This study offers valuable insights into enhancing the application of surfactant-based enhanced oil recovery techniques in medium- and low-permeability reservoirs.

#### 2. Experimental

#### 2.1. Materials

Acrylamide (AM, industrial-grade chemical) was sourced from Shandong Baomo Polymer Bioengineering Co., Ltd. (Dongying), 2acrylamide-2-methylpropane sulfonic acid (AMPS, 98%), methyl methacrylate octadecyl ester (SA, 96%), N,N-methylenebisacrylamide (MBA, 98%), Span type emulsifier, Tween type emulsifier, and anhydrous ethanol, all of the above reagents were acquired from Sinopsin Group Chemical Reagents Co., Ltd., Shanghai, China. Potassium persulfate and sodium bisulfite were obtained from Shanghai Chemical Reagent Co., Ltd., China. White oil, classified as industrial grade, was sourced from Dongying Shengli Chemical Co., Ltd., China. The crude oil used in the experiments, as well as the surfactant sodium alkyl alcohol polyoxyethylene ether carboxylate, was supplied by the Dongying Shengli Oilfield Technology Testing Center, China. NaCl, MgCl<sub>2</sub>, CaCl<sub>2</sub>, NaHCO<sub>3</sub>, and other chemicals were purchased from China National Pharmaceutical Group Chemical Reagent Co., Ltd. The simulated formation water used in the experiments was prepared in the laboratory, with total dissolved solids of 44592 mg/L. Its ion composition was as follows: 27004 mg/L Cl<sup>-1</sup>, 408 mg/L HCO<sub>3</sub>, 1760 mg/L Ca<sup>2+</sup>, 255 mg/L Mg<sup>2+</sup>, 15165 mg/L Na<sup>+</sup>.

#### 2.2. Experimental methods

#### 2.2.1. Synthesis of microspheres

The polymerization process of the microspheres is illustrated in Fig. 1. Initially, a blend of Span and Tween surfactants was used as the emulsifying agent. This blend was combined with hydrophobic monomers and white oil to form the oil phase. AM and AMPS were dissolved in water to serve as the water phase. The water and oil phases were then mixed and thoroughly stirred to form a W/O microemulsion.

The inverse microemulsion polymerization was conducted in a three-necked flask, with the initiator being added dropwise under continuous stirring. Throughout the reaction, nitrogen  $(N_2)$  was continuously purged to maintain an oxygen-free environment. The thermometer was used to monitor the exothermic process and temperature rise in real time. When the polymerization temperature stabilized, the reaction was allowed to continue for an additional 2-3 h to ensure complete polymerization of the microemulsion. The product was repeatedly precipitated and washed with ethanol to remove any residual emulsifier and oil phase, followed by drying at  $40\,^{\circ}\text{C}$  for 1 h to obtain the microsphere powder. The particle size distribution of the microspheres, both before and after swelling, was measured using a Mastersizer 3000 laser particle size analyzer.

#### 2.2.2. Preparation and stability analysis of emulsion

Simulated formation water was used to prepare mixed solutions of surfactant and microspheres at varying mass fractions. The mixed solutions were combined with crude oil at an oil-to-water volume ratio of 3:7 and placed in stoppered test tubes, then left

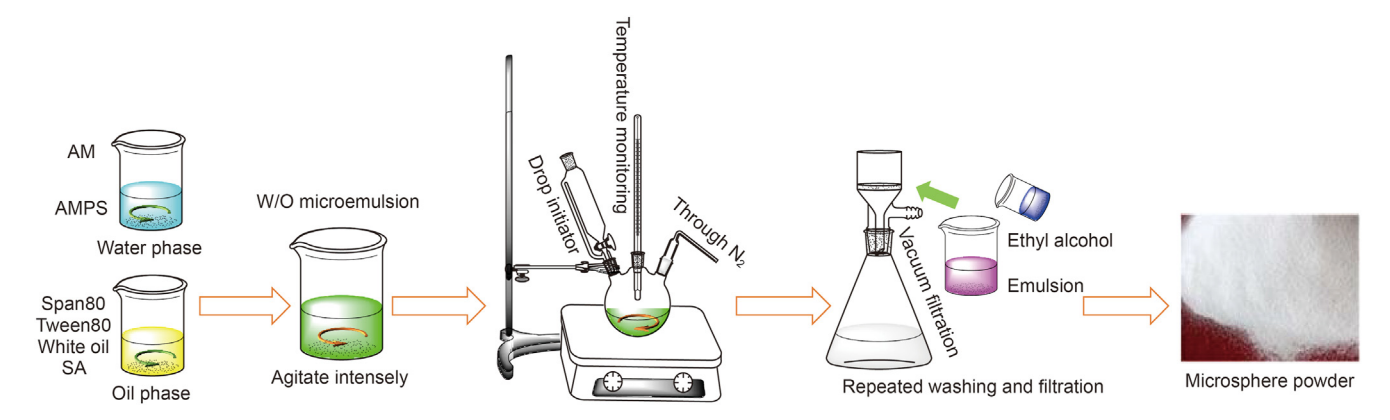


Fig. 1. Schematic diagrams of process.

to stand in a constant temperature oven at 80 °C for 30 min. After removing the samples, the stoppered tubes were gently inverted 180° five times to observe the dispersion of oil droplets in the water phase. The water separation rate of the emulsion was recorded over time, and the separation rate was calculated using Eq. (1).

$$f_{\rm W} = \frac{V_1}{V_0} \times 100\% \tag{1}$$

where  $f_{\rm w}$  denotes the water separation rate, %;  $V_{\rm 1}$  represents the volume of the lower water phase at various times, mL;  $V_{\rm 0}$  is the total volume of oil and water added, mL. The microstructure of the emulsions was observed using an XSJ-2 microscope, and the droplet size distribution was analyzed using Image J software.

#### 2.2.3. Sandpack plugging test

Artificial cores were employed to simulate the pore structure of the reservoir. The cores had a length of 10.0 cm, a diameter of 2.5 cm, and a permeability ranging from  $100 \times 10^{-3}$  to  $600 \times 10^{-3}$   $\mu m^2$ . The experimental apparatus is illustrated in Fig. 2.

Following the saturation of the core with simulated formation water, flow experiments using the microsphere/surfactant system were carried out at an injection rate of 0.2 mL/min and a temperature of 80 °C. Pressure changes were monitored throughout the experiment, and the permeability, plugging efficiency, resistance factor, and residual resistance factors were calculated using Eqs. (2)–(5).

$$k = \frac{Q\mu L}{A\Delta P_{\rm W}} \tag{2}$$

$$\eta = \frac{k_{\text{W1}} - k_{\text{W2}}}{k_{\text{W2}}} \tag{3}$$

$$F_{\rm R} = \frac{\Delta P_{\rm slug}}{\Delta P_{\rm initial}} \tag{4}$$

$$F_{\rm RR} = \frac{\Delta P_{\rm subsequent}}{\Delta P_{\rm initial}} \tag{5}$$

where k denotes the permeability of the core during the flow process; Q is the flow rate;  $\mu$  is the viscosity of the injected fluid; L is the core length; A represents the cross-sectional area of the core;  $\Delta P_{\rm w}$  is the pressure differential during the flow;  $\eta$  is the plugging efficiency of the microspheres;  $k_{\rm w1}$  and  $k_{\rm w2}$  are the permeabilities before and after plugging, respectively;  $F_{\rm R}$  and  $F_{\rm RR}$  denote the resistance factor and residual resistance factor, respectively;  $\Delta P_{\rm slug}$  refers to the pressure differential after the slug injection;  $\Delta P_{\rm subsequent}$  is the pressure differential during subsequent water flooding; and  $\Delta P_{\rm initial}$  is the pressure differential after stable water flooding. The oil displacement experiments were conducted under identical conditions.

#### 3. Results and discussion

#### 3.1. Optimization of microsphere synthesis conditions

#### 3.1.1. Preparation of reverse microemulsion

Microspheres were synthesized using a reverse microemulsion polymerization process. To enhance production efficiency, it is crucial to develop a uniform reverse microemulsion system with high solubilization capacity. A combination of Span and Tween

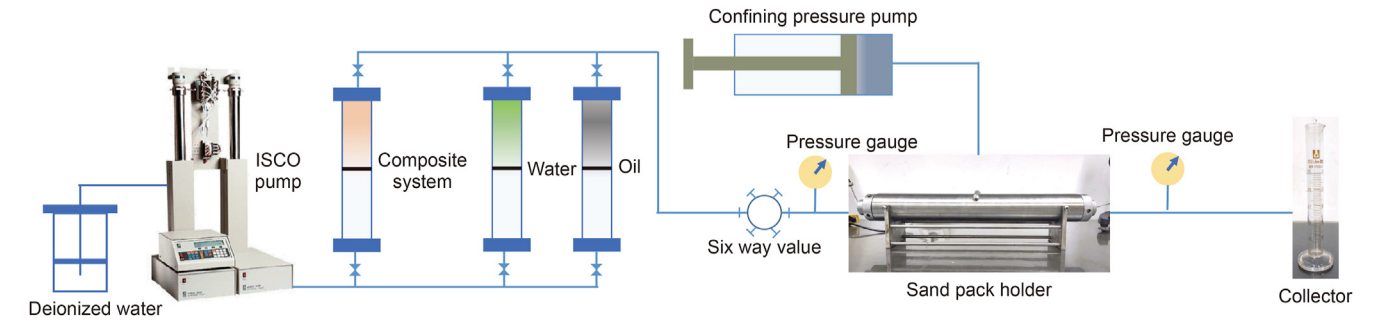


Fig. 2. Schematic diagram of core flooding experiments.

emulsifiers was employed, and the solubilization rate was optimized by adjusting the Span-to-Tween ratio, the emulsifier-towhite oil ratio, and the amount of sodium chloride added. Fig. 3(a) illustrates the solubilization performance of four emulsifier combinations at various ratios, with the emulsifier-to-oil ratio held constant at 1:2. The results show that for all Span + Tween emulsifier combinations, the solubilization rate increases initially and then decreases, reaching a peak at a Span-to-Tween ratio of 7:3. Among these, the Span80 + Tween80 combination exhibited the highest solubilization rate. Fig. 3(b) presents a ternary phase diagram for the emulsification system at a Span-to-Tween ratio of 7:3. The emulsion within region I, characterized by a specific oil-wateremulsifier ratio, forms a reversed-phase microemulsion, while the emulsion in region II no longer maintains this structure. The diagram further reveals that the Span80 + Tween80 combination achieved the highest solubilization rate of 32.5%, with the oil phase comprising 51% and the emulsifier making up 17%, resulting in an emulsifier-to-oil ratio of 1:3.

The addition of electrolytes aids in the formation of microemulsions. To further enhance the solubilization capacity of the water in the reverse microemulsion system, the oil-to-surfactant ratio was fixed at approximately 3:1, and an appropriate amount of sodium chloride was added to the system. Fig. 4 illustrates the effect of sodium chloride concentration on the water solubilization capacity of the system. As shown in Fig. 4, with increasing sodium chloride concentration, the solubilization capacity initially increases and then decreases. When the sodium chloride concentration reaches 1 wt%, the system achieves a maximum solubilization capacity of 42%. Through this optimization process, the system with the highest solubilization capacity was obtained when the Span-to-Tween ratio was 7:3, the surfactant-to-oil ratio was 1:3, and the sodium chloride concentration in the aqueous phase was 1 wt%.

#### 3.1.2. Optimization of polymerization reaction conditions

In the reverse microemulsion system with the highest water solubilization capacity, a microsphere polymerization reaction was carried out. Using the state of the microemulsion during the reaction as an indicator, the polymerization conditions were optimized through a single-factor variable control method.

The changes in the system state during the polymerization reaction, under the conditions of a reaction temperature of 25–40 °C,

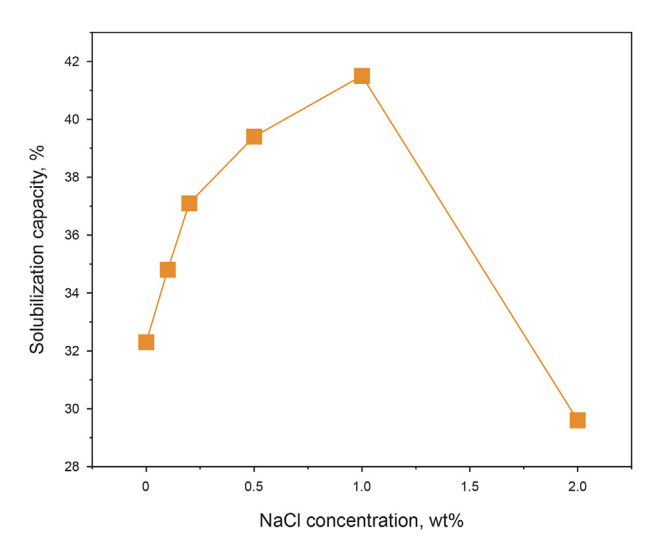


**Fig. 4.** Effect of sodium chloride concentration on water solubilization capacity of Span80 + Tween80 composite emulsion system.

a stirring speed of 500 rpm, and an initial initiator concentration of 0.10 wt% of the aqueous phase, are shown in Fig. 5(a). At lower temperatures, the polymerization reaction proceeds slowly, and the system temperature increases gradually. This is because the concentration of active free radicals is lower at low temperatures, leading to slower chain growth. As a result, the emulsion obtained is unstable, and phase separation occurs after stirring stops. This may be due to incomplete initiation at low temperatures, causing local polymerization of the monomer, which compromises the stability of the emulsion. On the other hand, when the temperature is too high, the polymerization reaction becomes intense, and the system temperature rises rapidly, resulting in a runaway polymerization of the monomer. At an initial polymerization temperature of 30–40 °C, a steady rise in reaction temperature was observed, and the final emulsion was semi-transparent.

Under the conditions of maintaining a temperature of  $35-40\,^{\circ}$ C, the effect of different stirring speeds on the reverse microemulsion polymerization was investigated. The results are shown in Fig. 5(b). At lower stirring speeds, noticeable gel blocks were formed during the reaction. This occurred because the low stirring speed

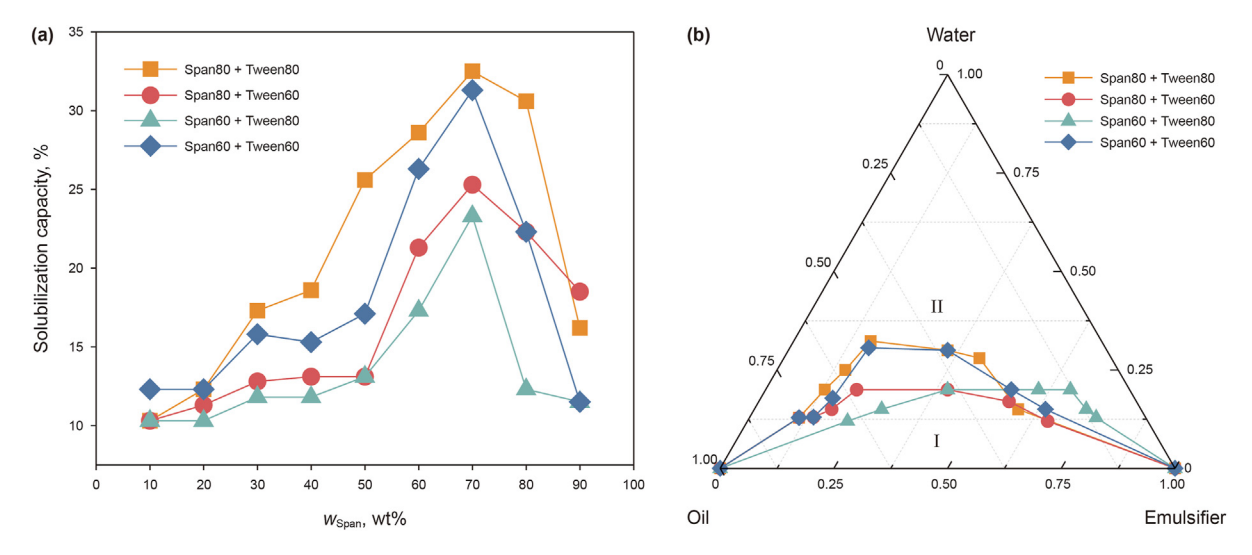


Fig. 3. Solubilization capacity of surfactant system at different compound ratios. (a) The ratio of emulsifier to oil phase was set at 1:2, while the proportion of Span and Tween type emulsifiers were varied. (b) The Span-to-Tween ratio was fixed at 7:3, while the proportion of emulsifier to oil phase were varied.

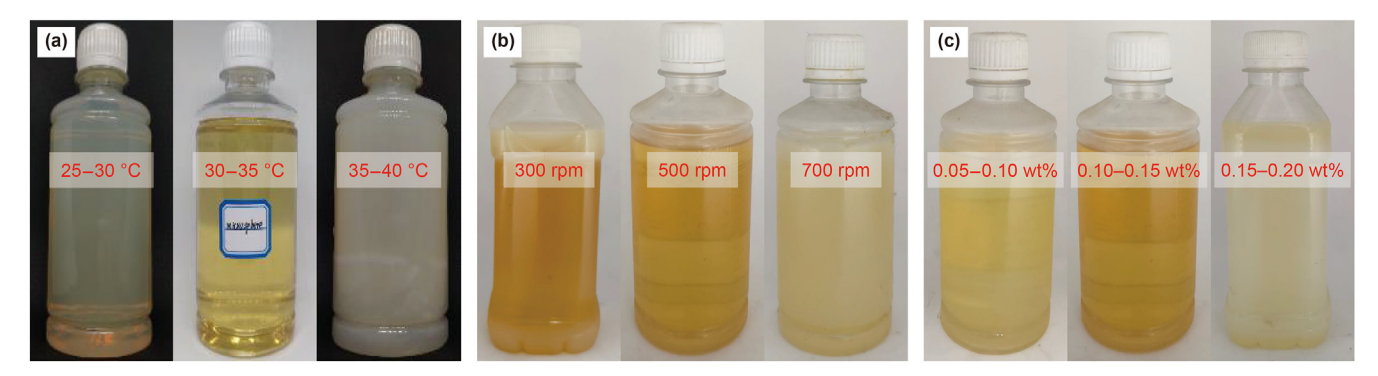


Fig. 5. State changes of emulsion under different reaction conditions. (a) Temperature; (b) stirring speed; (c) initiator concentration.

prevented the uniform distribution of the initiator solution throughout the emulsion, leading to a high local concentration of the initiator in some areas and a low concentration in others. As a result, some regions underwent intense reactions while others reacted more slowly. When the stirring speed was too high, the reaction system became unstable, with the emulsion turning turbid and making it difficult to monitor temperature changes. This instability may have been caused by the rapid release of free radicals and premature chain termination. At a stirring speed of 500 rpm, a steady increase in temperature was observed, and the emulsion remained relatively stable throughout the reaction.

Under the conditions of a stirring speed of 500 rpm and a temperature of 35–40 °C, the effect of initiator concentration on the polymerization reaction was further studied. The results are shown in Fig. 5(c). When the initiator concentration was low, the reaction proceeded slowly, the heating process was prolonged, and the final polymerization temperature remained relatively low. This resulted in phase separation of the product after standing. Conversely, when the initiator concentration was too high, the reaction occurred too quickly, and the system released heat rapidly, producing "white smoke" in the three-necked flask, and the final product became turbid. The optimal range of initiator concentration was found to be 0.10–0.15 wt%, within which the reaction proceeded at a moderate rate, the temperature rise was steady, and the monomer fully reacted.

After optimizing the initiation temperature, stirring speed, and initiator concentration, the optimal polymerization conditions were determined as an initiation temperature of 35–40 °C, a stirring speed of 500 rpm, and an initiator concentration of 0.10–0.15 wt%. The particle size of the synthesized microspheres was characterized, and the results are shown in Fig. 6. As seen in Fig. 6(a), the initial microsphere size ranged from 200 to 800 nm, with a  $D_{50}$  of 400 nm. As shown in Fig. 6(b), after reaching swelling equilibrium, most of the microspheres had a particle size distribution in a range of 1–3  $\mu$ m, with a  $D_{50}$  of 2  $\mu$ m and a swelling ratio of approximately 5 times.

### 3.2. Stability of the microsphere/murfactant composite system emulsion

The emulsification performance of microspheres in synergy with surfactants was evaluated, and the water separation rates of emulsions under different surfactant and microsphere concentrations were tested, as shown in Fig. 7. Fig. 7(a) illustrates that, without the addition of microspheres, the emulsifying ability of the surfactant under hand-shaking conditions was poor. When the surfactant concentration ranged from 0.10 to 0.30 wt%, after shaking five times, the initial water separation rate of the emulsion exceeded 70%, reaching 100% within 5 min. As the surfactant

concentration increased to 0.40 wt%, the emulsion stability slightly improved, with an initial water separation rate of around 20%, but complete demulsification occurred within 10 min. When the surfactant concentration was further increased to 0.60 wt%, the emulsion stability improved, but the effect was minimal, with an initial water separation rate of about 5%, and complete demulsification occurred within 30 min.

With the surfactant concentration fixed at 0.40 wt%, the effect of microsphere concentration on the water separation rate of the emulsion was examined, as shown in Fig. 7(b). When the microsphere concentration was 0.05 wt%, the stability of the emulsion significantly improved. As the microsphere concentration increased, at 0.20 wt%, the initial water separation rate was 0, and after 30 min, the water separation rate was only 23%. Complete demulsification occurred after 2 h, with the water separation rate reaching 100%. Fig. 8 further demonstrates the enhancement of emulsion stability with the addition of microspheres. It is important to note that when the microsphere concentration was increased beyond this point, the stability of the emulsion actually decreased. This may be due to interactions between the hydrophobic monomers on the microsphere surface and the hydrophobic ends of the surfactant, causing surfactant aggregation at the oil-water interface, which affected the adsorption behavior of surfactant at the interface (Jiang et al., 2016).

To further understand the effect of microspheres on emulsion stability, the microscopic morphology of the emulsion was observed before and after the addition of microspheres using a microscope. The changes in emulsion droplet size were also analyzed, as shown in Fig. 9. It is evident that the addition of microspheres resulted in a more uniform droplet size. Further analysis of the droplet size distribution before and after the addition of microspheres, as shown in Fig. 9(c) and (d), revealed that before adding microspheres, most droplets had diameters greater than 10  $\mu m$ , with a wide size distribution ranging from approximately 5  $\mu m$  to over 40  $\mu m$ . After the addition of microspheres, the droplet size was primarily concentrated between 5 and 8  $\mu m$ , with a narrower size distribution. This indicates that the addition of microspheres helped reduce droplet size and improved the adsorption of surfactants at the emulsion interface.

#### 3.3. Enhanced oil recovery performance

#### 3.3.1. Plugging ability of microspheres in porous media

The seepage ability of the microsphere solution in the core was tested, as illustrated in Fig. 10. At an injection rate of 0.2 mL/min, the pressure in the sand-packed tube stabilized after approximately 1.5 pore volumes (PV) of water flooding. Upon switching to the composite system, the pressure began to fluctuate and eventually stabilized at a certain level. As the permeability increased, the

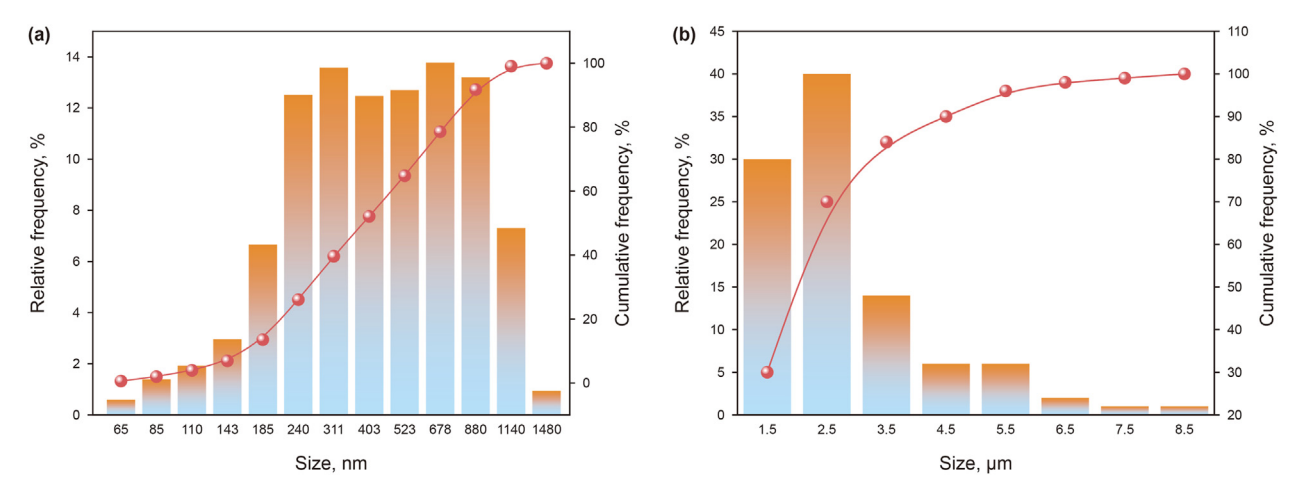


Fig. 6. Particle size distribution of active microspheres before swelling (a) and at swelling equilibrium (b).

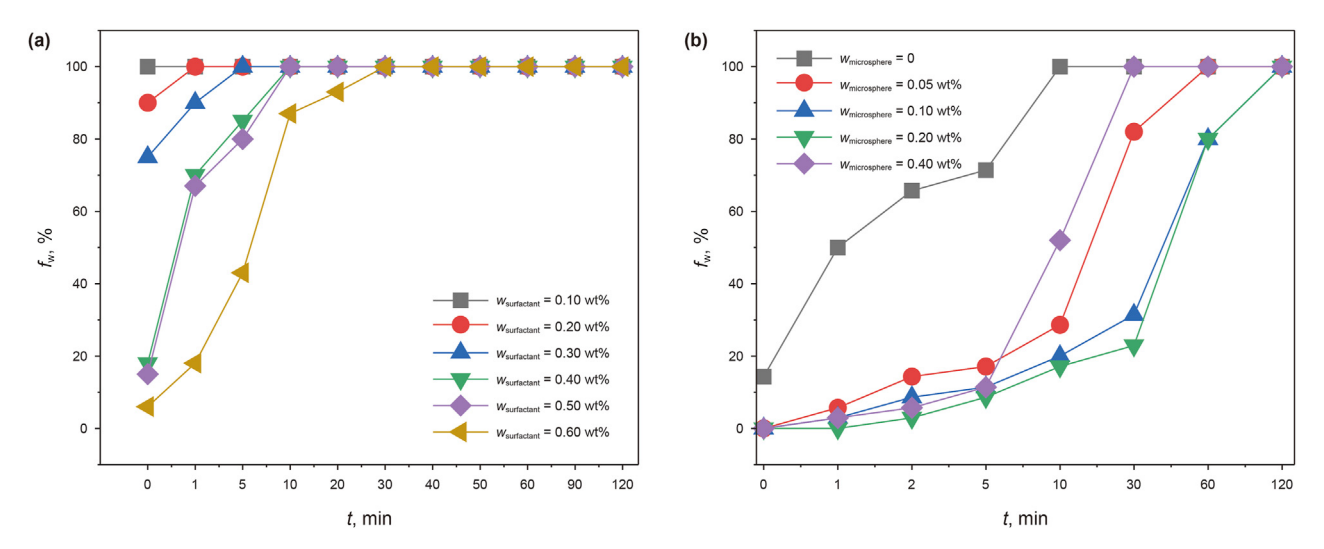


Fig. 7. Effects of surfactant (without the addition of microspheres) (a) and microsphere (the surfactant concentration fixed at 0.4 wt%) (b) concentrations on water separation rate of emulsion.

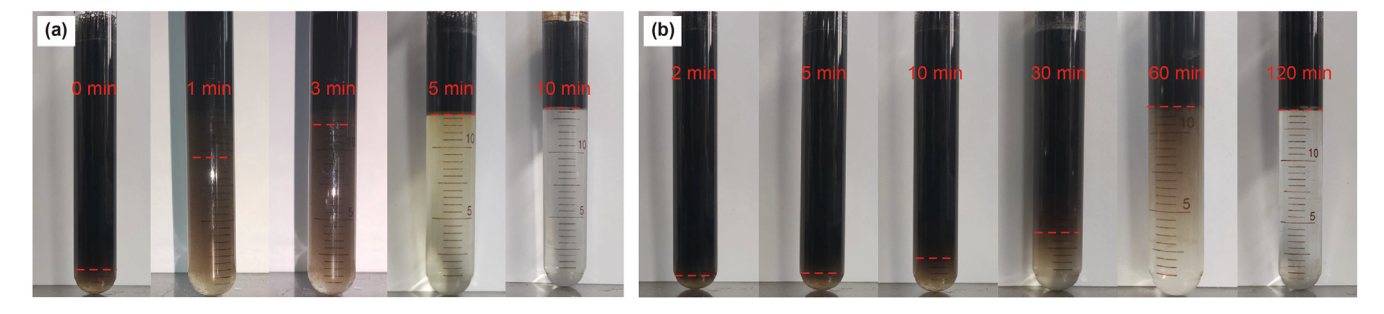


Fig. 8. Stability of emulsions before (a) and after (b) the addition of microspheres (the surfactant concentration fixed at 0.40 wt%).

stable pressure gradually decreased. During subsequent water flooding, the pressure continued to decrease and eventually stabilized. The experimental observations suggest that the adsorption and bridging of microspheres in narrow pores caused some blockage, resulting in increased pressure. However, when the pressure became too high, the weak blockage created by the microspheres was dispersed by the water flow. Additionally, microspheres may have caused further blockage in even narrower pore

throats during their movement. This cyclic process of blockage-migration-blockage led to persistent pressure fluctuations. During the subsequent water flooding process, the absence of continuous injection of fresh microsphere solution led to a gradual decrease in microsphere concentration. Some microspheres with smaller diameters were likely flushed out of the core, causing the pressure to drop and then stabilize at a certain value.

The resistance factor and residual resistance factor after

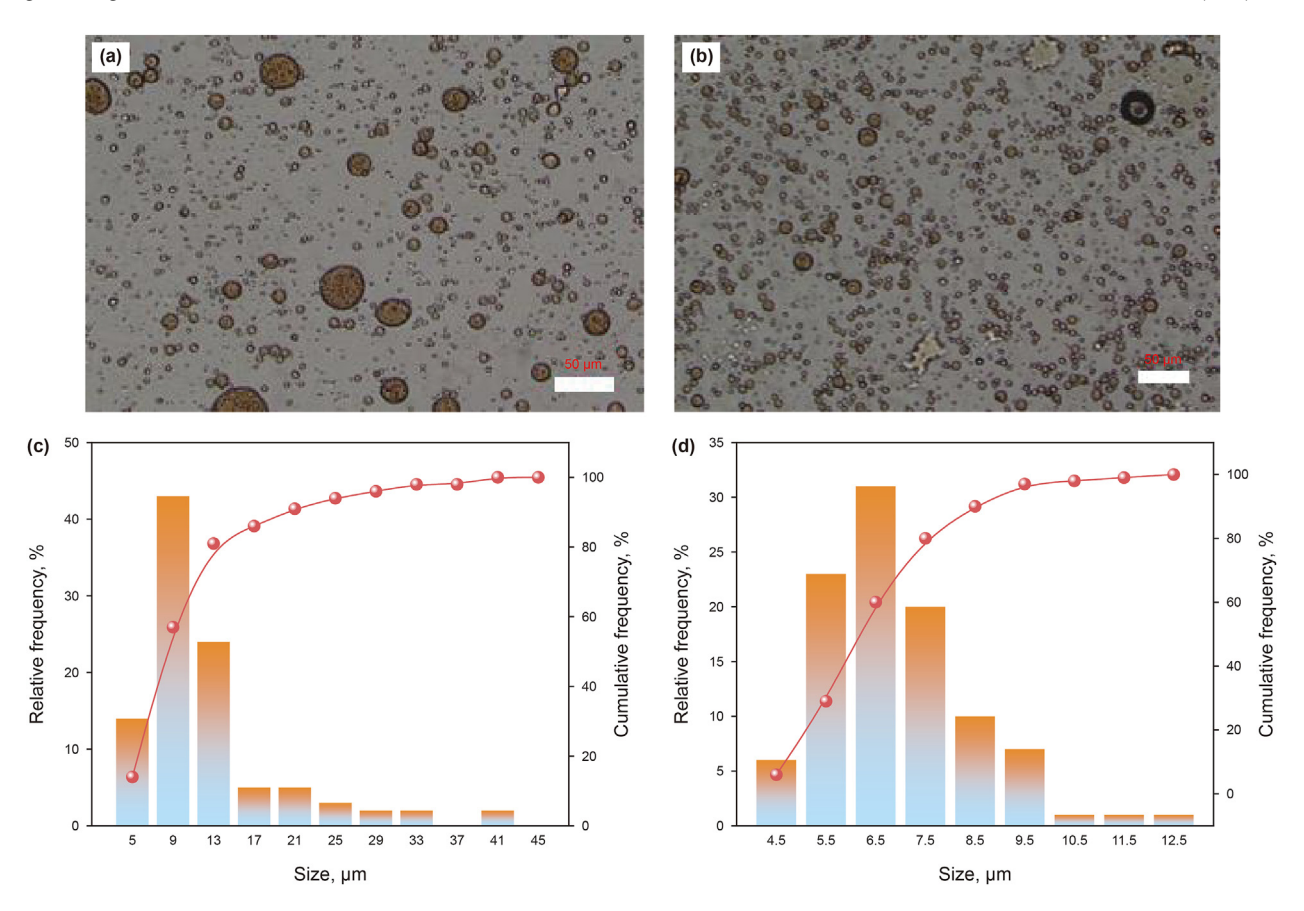


Fig. 9. The microemulsion morphology of emulsions before (a) and after (b) the addition of microspheres; and particle size distributions of emulsions before (c) and after (d) the addition of microspheres.

microsphere injection at different permeabilities were calculated, as shown in Table 1. The injection of microspheres significantly affected the core permeability, with resistance factors ranging from 30 to 60 and residual resistance factors from 10 to 20. This indicates that microsphere injection created some degree of blockage within the porous medium. During subsequent water flooding, a decrease in pressure was observed, which may be due to the flushing effect of the water flow causing some microspheres to be displaced from the core. However, a portion of the microspheres remained within the core, resulting in an effective blocking effect.

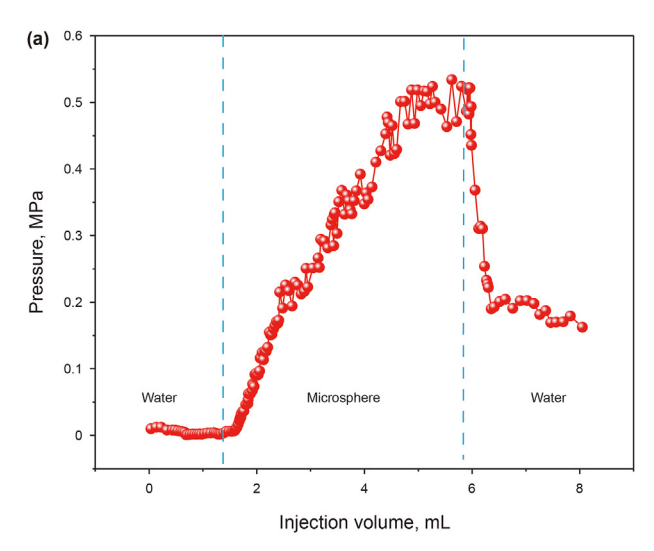
Further calculations were performed to evaluate the variation in blocking efficiency during subsequent water flooding at different permeabilities, as shown in Fig. 11. The blocking efficiency in cores with different permeabilities was consistently above 90%, indicating that microspheres generally exhibit excellent blocking performance. As water flooding progressed, the blocking efficiency of the cores with permeabilities of 309  $\times$  10<sup>-3</sup> and 523  $\times$  10<sup>-3</sup>  $\mu m^2$ initially decreased and then stabilized. This suggests that microspheres formed a relatively stable blocking structure within the core that was resistant to disruption under limited flushing conditions. In contrast, for the core with a permeability of  $112 \times 10^{-3} \, \mu \text{m}^2$ , the blocking efficiency continuously decreased, indicating an unstable blocking effect. This may be because the lower permeability causes a high concentration of microspheres at the core inlet, preventing microspheres from effectively migrating into the deep section of the core. Consequently, only a few microspheres entered the core and moved with the water flow, resulting in weaker bridging and adsorption effects.

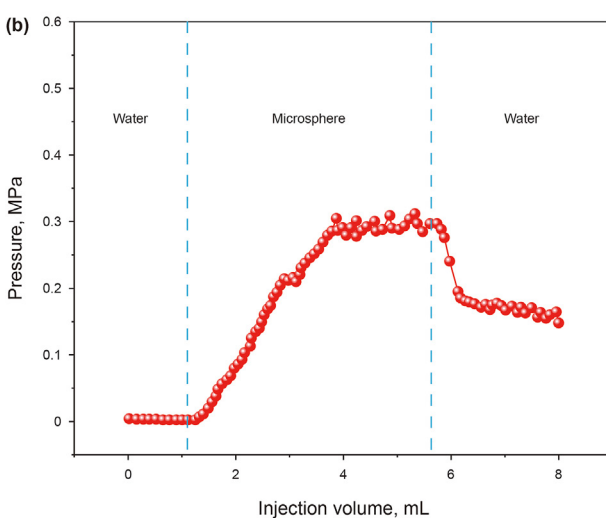
To further investigate the profile control effect of microspheres in heterogeneous reservoirs, we designed a parallel-core

displacement experiment with a flow rate of 0.2 mL/min. The experimental results are shown in Fig. 12. It is evident from the figure that during the initial water flooding stage, the flow rate through the high-permeability core is higher than that through the low-permeability core, and the injection pressure is also lower. In the composite system injection stage, microspheres preferentially enter the high-permeability core due to the significantly higher flow pressure in the low-permeability core compared to the highpermeability core. This results in a temporary increase in flow rate through the high-permeability core and a decrease in flow rate through the low-permeability core, with some microsphere accumulation observed at the entrance of the low-permeability core. As the distance traveled by microspheres in the high-permeability core increases, the required flow pressure also increases. The effective permeability of the high-permeability core gradually decreases, leading to its blockage. During the subsequent water flooding stage, the effective permeability of the high-permeability core decreases while that of the low-permeability core remains relatively unchanged. The flow diversion rate in the lowpermeability core reaches 90%, with water primarily flowing through the low-permeability core. This indicates that with a permeability ratio of 3, microspheres can alter the flow direction of the liquid and help increase the sweep volume of the surfactant.

## 3.3.2. The enhanced oil recovery effect of the microsphere/surfactant composite system

The enhanced oil recovery capabilities of two systems, namely the surfactant system and the microsphere/surfactant composite system, were evaluated. The experimental setup was shown in Fig. 2, with an injection rate of 0.2 mL/min. As shown in Fig. 13,





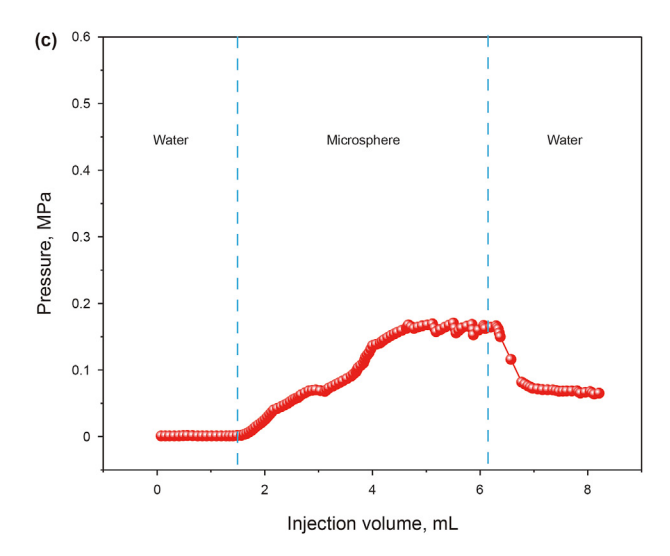


**Fig. 10.** The seepage pressure curves of homogeneous single core under different permeability. (a)  $112 \times 10^{-3} \ \mu m^2$ ; (b)  $309 \times 10^{-3} \ \mu m^2$ ; (c)  $523 \times 10^{-3} \ \mu m^2$ .

during the water flooding stage, as the injected volume increased, both the oil recovery and water cut gradually rose, peaked and then stabilized over time. After switching to surfactant injection, the water cut decreased and the oil recovery increased. This was

**Table 1**Resistance factor and residual resistance factor of homogeneous single core under different permeability.

k, 10 <sup>-3</sup> μm <sup>2</sup>	$\Delta P_{ m initial}$ , MPa	$\Delta P_{\rm slug}$ , MPa	$\Delta P_{ m subsequent}$ , MPa	$F_{\rm R}$	$F_{\rm RR}$
112	0.015	0.49	0.18	33	12
309	0.005	0.29	0.16	58	32
523	0.003	0.15	0.07	50	23

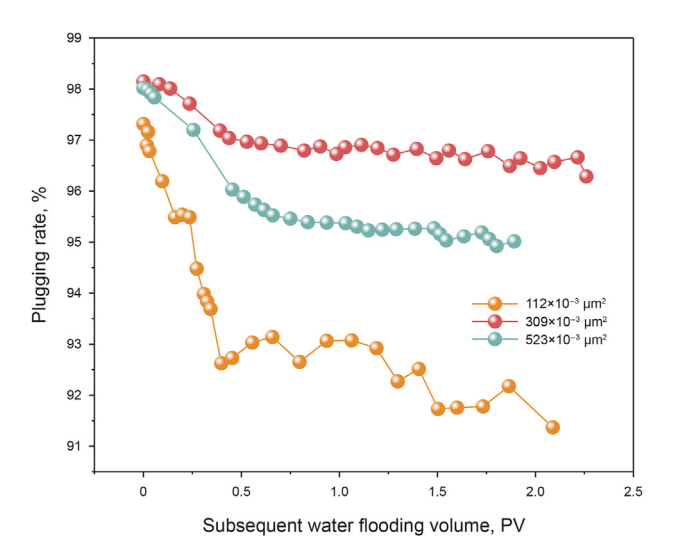


Fig. 11. Change of plugging rate in subsequent water flooding process.

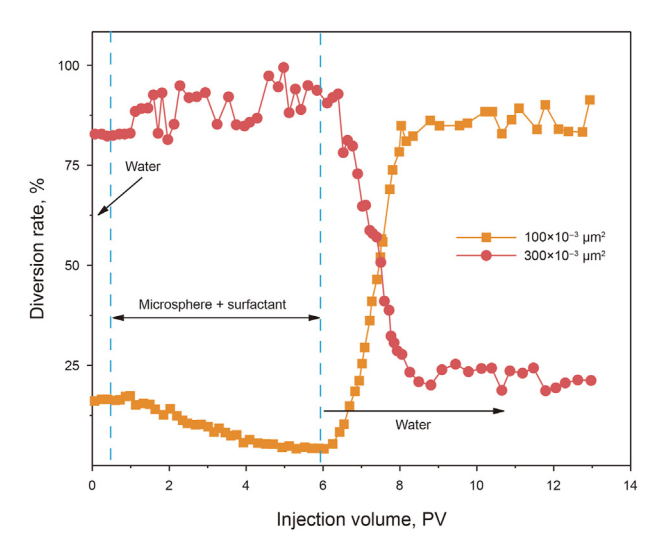


Fig. 12. Diversion rate of composite system in the parallel-core model.

because, after the surfactant was injected into the core, the fluid experienced shear forces in the pore throats and formed an emulsion under the effluence of surfactant. During flow, the emulsion blocked the pore throats due to the Jamin effect, which increased the sweep efficiency and significantly reduced the water cut. Additionally, the surfactant reduced the interfacial tension, enhancing oil washing efficiency and thus increasing oil recovery. Notably, as shown in Fig. 14, the oil recovery rate of the single surfactant system decreased gradually with increasing permeability. This was attributed to the weaker shear effect between the chemicals and oil droplets in the porous medium at intermediate to high permeabilities, which resulted in unstable emulsions and less

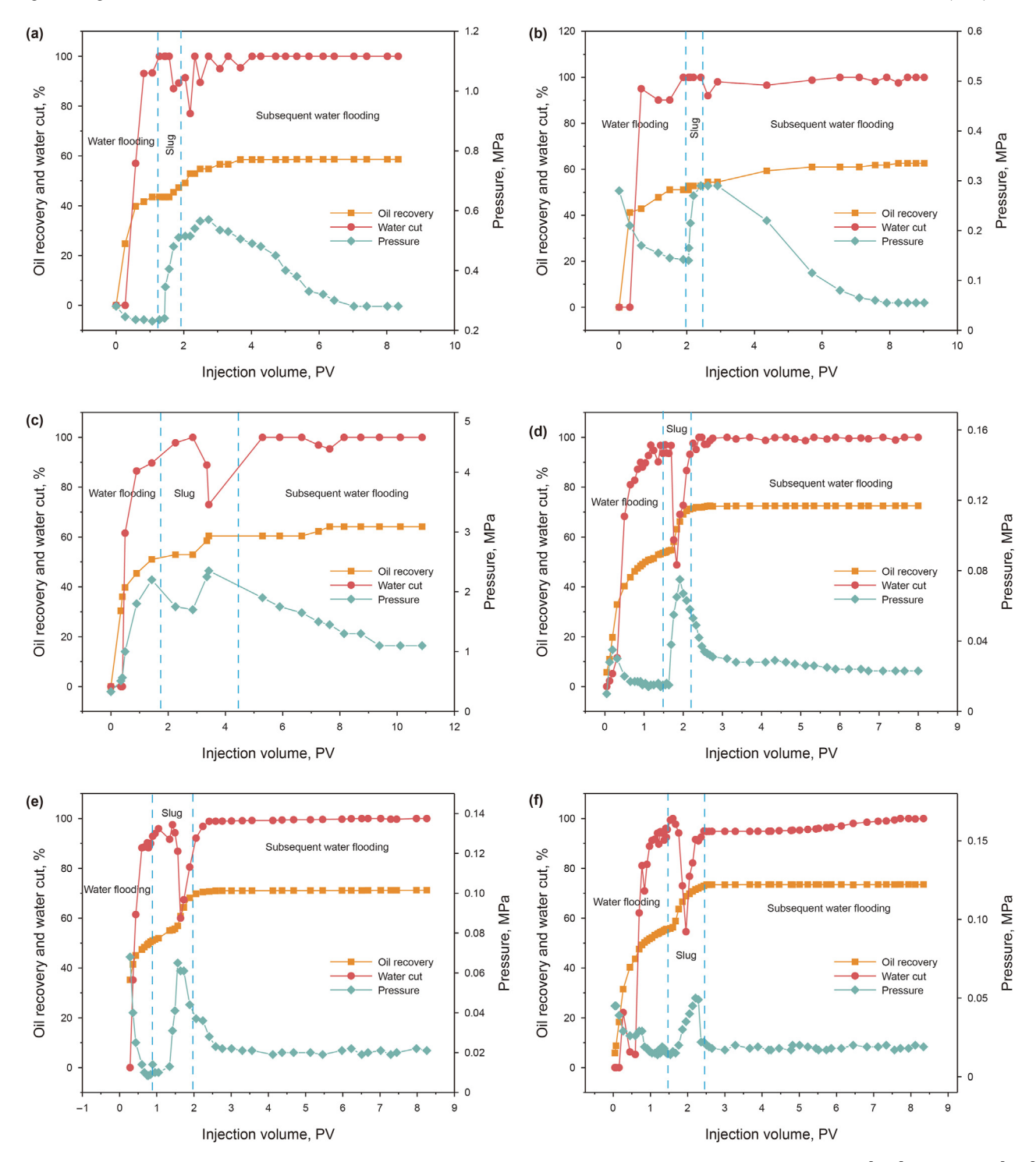


Fig. 13. Changes of water cut and recovery efficiency during injection of composite system fluid into different permeability cores. (a)  $140 \times 10^{-3} \, \mu m^2$ ; (b)  $334 \times 10^{-3} \, \mu m^2$ ; (c)  $574 \times 10^{-3} \, \mu m^2$ ; (d)  $136 \times 10^{-3} \, \mu m^2$ ; (e)  $326 \times 10^{-3} \, \mu m^2$ ; (f)  $523 \times 10^{-3} \, \mu m^2$ .

effective oil recovery in low interfacial tension systems. In contrast, the microsphere/surfactant composite system demonstrated a more pronounced reduction in water cut and a more significant improvement in oil recovery after switching to injection. At different permeabilities, the composite system increased oil recovery by 4.5%, 8.3%, and 4.8%, respectively, compared to the single system. This indicated that the composite system exhibited a strong synergistic effect, which became more pronounced with increasing permeability. The addition of microspheres stabilizes the in-situ

emulsion and plugs the high-permeability flow channels through adsorption and retention in the pore throat, expanding the sweep efficiency and improving the recovery factor. When the permeability is  $140\times10^{-3}~\mu\text{m}^2$ , the formation exhibits strong shear ability, allowing the surfactant slug alone to form a relatively stable in-situ emulsion, in which case the synergistic stabilization effect of the microspheres is not fully realized. As the permeability increases to  $330\times10^{-3}~\mu\text{m}^2$ , both the synergistic stabilization effect of the microspheres and their adsorption and retention effects are

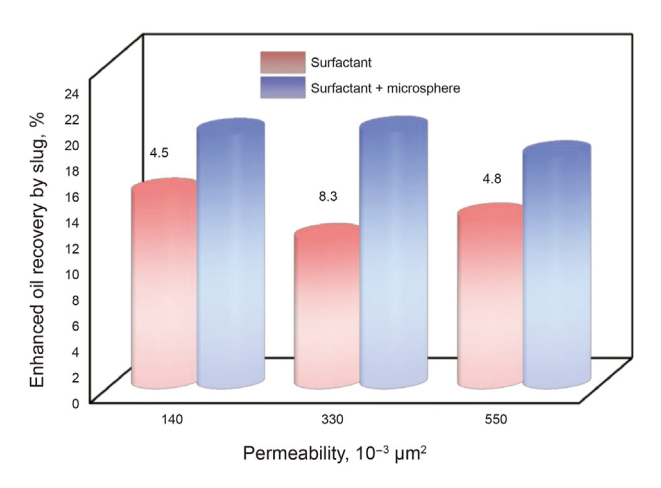


Fig. 14. Enhanced oil recovery using different slug at different permeability.

significantly enhanced, resulting in the greatest increase in recovery factor with the composite slug. However, when the permeability further increases to  $550\times10^{-3}~\mu\text{m}^2$ , the blocking capacity of the microspheres declines, leading to a reduced increase in recovery factor. Overall, the improvement in composite slug flooding efficiency is attributed to both the enhanced stability of the emulsion and the blocking effect of the microspheres in the porous medium, both of which are closely related to the core permeability.

#### 4. Conclusions

This study prepared microspheres using AM, AMPS, and SA as basic monomers, with MBA as a crosslinking agent. These microspheres were then used in conjunction with a surfactant that possesses micro-dynamic emulsification properties to enhance the oil recovery effectiveness of surfactant.

- (1) A stable microemulsion system was prepared using the maximum water solubilization rate as the indicator, and the polymerization conditions for microspheres were determined by monitoring the reaction state. Particle size distribution analysis showed that the initial microsphere size ranged from 200 to 800 nm, with a  $D_{50}$  of 400 nm. After reaching swelling equilibrium, the particle size was  $1-3~\mu m$ , with a  $D_{50}$  of 2  $\mu m$ , and the swelling rate was approximately 5 times.
- (2) The microsphere/surfactant composite system significantly improved emulsion stability. With the addition of only 0.4 wt% surfactant, the initial water separation rate of the emulsion was about 20%, and complete demulsification occurred within 10 min. After adding 0.2 wt% microspheres, the initial water separation rate dropped to 0, with only 23% separation after 30 min, and complete demulsification taking 2 h. Additionally, the microspheres made the droplet size more uniform, as observed in the microstructure analysis.
- (3) The injection of microspheres significantly affects the permeability of the core. Under varying permeability conditions, the resistance coefficients after microsphere injection ranged from 30 to 60, with residual resistance coefficients of 10–20, and the plugging efficiencies exceeding 90%. Oil displacement experiments demonstrated that the microsphere/surfactant composite system achieved a significantly higher enhanced oil recovery compared to the single surfactant system. At different permeability levels, the increases in oil recovery rates for the composite system compared to the single system were 4.5%, 8.3%, and 4.8%, respectively.

#### **CRediT authorship contribution statement**

**Yu-Hui Yang:** Writing — original draft, Methodology, Data curation. **Chu-Yu Kang:** Writing — review & editing, Supervision, Investigation. **Ting-Feng Liu:** Resources. **Hang Li:** Software, Formal analysis. **Hui-Min Yu:** Visualization, Methodology. **Zhuo-Zhuang Liu:** Validation. **Hai-Ming Fan:** Funding acquisition, Conceptualization.

#### **Declaration of competing interest**

The authors declare that they have no known competing financial interests or personal relationships that could have appeared to influence the work reported in this paper.

#### Acknowledgment

This work was supported by the Natural Science Foundation of Shandong Province (ZR2021ME007), the National Natural Science Foundation in China (51574267), and the Key Projects of China National Key Research and Development Plan (2019YFA0708703).

#### References

- An, Y., Yao, X., Zhong, J., et al., 2022. Enhancement of oil recovery by surfactant-polymer synergy flooding: a review. Polym. Polym. Compos. 30. https://doi.org/10.1177/09673911221145834.
- Arab, D., Kantzas, A., Bryant, S.L., 2018. Nanoparticle stabilized oil in water emulsions: a critical review. J. Petrol. Sci. Eng. 163, 217–242. https://doi.org/10.1016/j.petrol.2017.12.091.
- Baek, K.H., Argielles-Vivas, F.J., Okuno, R., et al., 2019. An experimental study of emulsion phase behavior and viscosity for athabasca bitumen/diethylamine/ brine mixtures. SPE Reservoir Eval. Eng. 22, 628-641. https://doi.org/10.2118/ 180768. DA
- Bai, Y., Wang, Z., Shang, X., et al., 2017. Experimental evaluation of a surfactant/compound organic alkalis flooding system for enhanced oil recovery. Energy Fuels 31, 5860–5869. https://doi.org/10.1021/acs.energyfuels.7b00322.
- Chen, L., Huang, F., Li, G., et al., 2023. Experimental study on fiber balls for bridging in fractured-vuggy reservoir. SPE J. 28, 1880–1894. https://doi.org/10.2118/214315-PA.
- Dantas, T.N.D.C.De, Oliveira, A.C.D.E., Souza, T.T.C., et al., 2020. Experimental study of the effects of acid microemulsion flooding to enhancement of oil recovery in carbonate reservoirs. Journal of Petroleum Exploration and Production Technology 10. 1127—1135. https://doi.org/10.1007/s13202-019-00754-x.
- Fan, H.C., Pu, W.F., Du, D.J., et al., 2023. Experimental study on the plugging and profile control of preformed particle gels in high temperature and salinity reservoir. J. Appl. Polym. Sci. 140 (32), e54247. https://doi.org/10.1002/app.54247.
- Hou, X.Y., Sheng, J.J., 2022. Fabrication of a spontaneous emulsification system for low-permeable oil reservoirs and study of an enhanced oil recovery mechanism based on the nuclear magnetic resonance method. Energy Fuels 36, 227–238. https://doi.org/10.1021/acs.energyfuels.1c03187.s001.
- https://doi.org/10.1021/acs.energyfuels.1c03187.s001.

  Jiang, J.T., Kang, X., Wu, H.R., et al., 2021. Spontaneous emulsification induced by a novel surfactant-polymer compound system and its application to enhance oil recovery. J. Mol. Liq. 337. https://doi.org/10.1016/j.molliq.2021.116399.
- Jiang, L., Li, S., Yu, W., et al., 2016. Interfacial study on the interaction between hydrophobic nanoparticles and ionic surfactants. Colloids Surf. A Physicochem. Eng. Asp. 488, 20–27. https://doi.org/10.1016/j.colsurfa.2015.10.007.
- Kumar, G., Kakati, A., Mani, E., et al., 2021. Stability of nanoparticle stabilized oil-in-water Pickering emulsion under high pressure and high temperature conditions: comparison with surfactant stabilized oil-in-water emulsion. J. Dispersion Sci. Technol. 42, 1204–1217. https://doi.org/10.1080/01932691.2020.1730888.
- Lee, J., Huang, J., Babadagli, T., 2020. Dynamics of emulsion generation and stability during heavy oil displacement with chemicals and nanoparticles: qualitative analysis using visual 2D data. Fuel 270. https://doi.org/10.1016/ifuel 2020 117502
- Li, G., Ruan, Y., Chen, L.F., et al., 2019. Alkyl polyglycoside: a green and efficient surfactant for enhancing heavy oil recovery at high-temperature and highsalinity condition. J. Pet. Explor. Prod. Technol. 9 (4), 2671–2680. https:// doi.org/10.1007/s13202-019-0658-1.
- Li, X., Zhang, X., Zhang, Y., et al., 2022. Polystyrene nanofluids for enhanced oil recovery. Colloids Surf. A Physicochem. Eng. Asp. 649. https://doi.org/10.1016/ i.colsurfa.2022.129399.
- Li, Z., Kang, W.L., Bai, B.J., et al., 2019. Fabrication and mechanism study of the fast spontaneous emulsification of crude oil with anionic/cationic surfactants as an enhanced oil recovery (EOR) method for low-permeability reservoirs. Energy Fuel. 33, 8279–8288. https://doi.org/10.1021/acs.energyfuels.9b01796.

- Liu, J., Zhong, L., Hao, T., et al., 2022. A collaborative emulsification system capable of forming stable small droplets of oil-in-water emulsions for enhancing heavy oil recovery. J. Mol. Liq. 355. https://doi.org/10.1016/j.molliq.2022.118970.
- Liu, X.M., Chen, Z., Cui, Z.G., 2021. Fatty alcohol polyoxyethylene ether sulfonate for foam flooding in high-salinity and high-temperature reservoir conditions. Colloids Surf. A Physicochem. Eng. Asp. 629. https://doi.org/10.1016/ j.colsurfa.2021.127366.
- Lu, J., Goudarzi, A., Chen, P.L., et al., 2014. Enhanced oil recovery from high-temperature, high-salinity naturally fractured carbonate reservoirs by surfactant flood. J. Petrol. Sci. Eng. 124, 122–131. https://doi.org/10.1016/i.petrol.2014.10.016.
- Ma, X., Zhou, Y., Yi, P., et al., 2022. Design, preparation and properties of new polyacrylamide based composite nano-microspheres with like "ball in ball" structure. Colloids Surf. A Physicochem. Eng. Asp. 654. https://doi.org/10.1016/ i.colsurfa.2022.130037.
- Saha, R., Uppaluri, R.V.S., Tiwari, P., 2018. Effects of interfacial tension, oil layer break time, emulsification and wettability alteration on oil recovery for carbonate reservoirs. Colloids Surf. A Physicochem. Eng. Asp. 559, 92–103. https://doi.org/ 10.1016/j.colsurfa.2018.09.045.
- Saha, R., Sharma, A., Uppaluri, R.V.S., et al., 2019. Interfacial interaction and emulsification of crude oil to enhance oil recovery. Int. J. Oil Gas Coal Technol. 22, 1–15. https://doi.org/10.1504/ijogct.2018.10011553.
- Shang, X., Bai, Y., Sun, J., et al., 2019. Performance and displacement mechanism of a surfactant/compound alkaline flooding system for enhanced oil recovery. Colloids Surf. A Physicochem. Eng. Asp. 580. https://doi.org/10.1016/ j.colsurfa.2019.123679.
- Sharma, V.K., Singh, A., Tiwari, P., 2023. An experimental study of pore-scale flow dynamics and heavy oil recovery using low saline water and chemical flooding.

- Fuel 334. https://doi.org/10.1016/j.fuel.2022.126756.
- Wang, J., Kang, W., Yang, H., et al., 2022. Study on salt tolerance mechanism of hydrophobic polymer microspheres for high salinity reservoir. J. Mol. Liq. 368. https://doi.org/10.1016/j.molliq.2022.120639.
- Wang, Z., Hu, R., Ren, G., et al., 2019. Polyetheramine as an alternative alkali for alkali/surfactant/polymer flooding. Colloids Surf. A Physicochem. Eng. Asp. 581. https://doi.org/10.1016/j.colsurfa.2019.123820.
- Wang, Z., Lin, M., Jin, S., et al., 2020. Combined flooding systems with polymer microspheres and nonionic surfactant for enhanced water sweep and oil displacement efficiency in heterogeneous reservoirs. J. Dispersion Sci. Technol. 41, 267–276. https://doi.org/10.1080/01932691.2019.1570850.
- Zhao, L., Qin, B., Wu, X.J., et al., 2021. Study on reducing injection pressure of low permeability reservoirs characterized by high temperature and high salinity. China Pet. Process. Petrochem. Technol. 23, 44–54 (in Chinese).
- Zheng, L., Wang, H., Zhang, Y., et al., 2022. Experimental study on water-plugging performance of silicon dioxide/polystyrene hydrophobic insoluble microsphere particle flooded by high-water-cut oil-water mixture. Journal of Energy Resources Technology-Transactions of the Asme 144. https://doi.org/10.1115/ 14054702
- Zhou, R., Zhang, D., Tao, J., et al., 2022. New insight to experimental study on pore structure of different type reservoirs during alkaline-surfactant-polymer flooding. Energy Sci. Eng. 10, 2527–2539. https://doi.org/10.1002/ese3.1206.
- Zhou, Y., Luo, Z., Xu, M., et al., 2023. Preparation and properties of temperaturesensitive P(NIPAM-AM) Nano-microspheres in enhanced oil recovery. Energy Fuels 37, 204–213. https://doi.org/10.1021/acs.energyfuels.2c02972.s001.
- Zhu, J.J., Yang, L., Zhao, K., et al., 2022. Performance evaluation and mechanism study of environment-friendly polymer microspheres/surfactant composite flood control system. Fresenius Environ. Bull. 31 (10), 10375–10382.